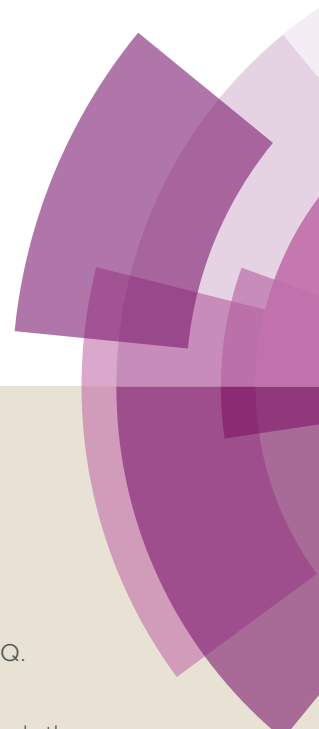


Journal of Materials Chemistry C

Accepted Manuscript



This article can be cited before page numbers have been issued, to do this please use: X. Yuan, M. Yu, Q. Zhu, W. Zhang, L. Xie, W. Huang and J. Ma, *J. Mater. Chem. C*, 2018, DOI: 10.1039/C7TC04817C.



This is an Accepted Manuscript, which has been through the Royal Society of Chemistry peer review process and has been accepted for publication.

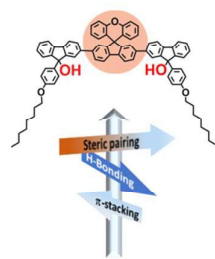
Accepted Manuscripts are published online shortly after acceptance, before technical editing, formatting and proof reading. Using this free service, authors can make their results available to the community, in citable form, before we publish the edited article. We will replace this Accepted Manuscript with the edited and formatted Advance Article as soon as it is available.

You can find more information about Accepted Manuscripts in the [author guidelines](#).

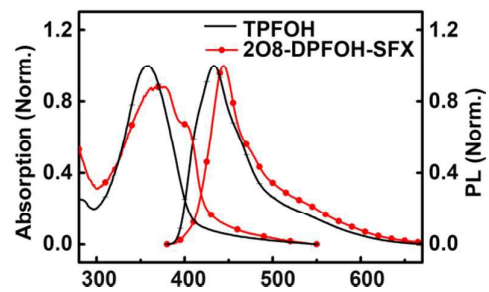
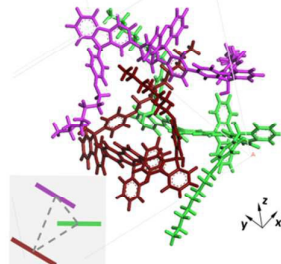
Please note that technical editing may introduce minor changes to the text and/or graphics, which may alter content. The journal's standard [Terms & Conditions](#) and the ethical guidelines, outlined in our [author and reviewer resource centre](#), still apply. In no event shall the Royal Society of Chemistry be held responsible for any errors or omissions in this Accepted Manuscript or any consequences arising from the use of any information it contains.

Table of Contents

208-DPFOH-SFX



raceme



Synergistic Steric Pairing Effects of Terfluorenes with Ternary Side Groups on β -Conformation Transition: Experiments and Computations

Xiang-Ai Yuan,^{1,†} Meng-Na Yu^{2,†}, Qiang Zhu,¹ Wan-Wan Zhang,² Ling-Hai Xie,^{2,} Wei Huang,² Jing Ma^{1,*}*

¹Key Laboratory of Mesoscopic Chemistry of MOE School of Chemistry & Chemical Engineering, Nanjing University, 22 Hankou Road, Nanjing, 210093, People's Republic of China

²Center for Molecular Systems & Organic Devices (CMSOD), Key Laboratory for Organic Electronics and Information Displays & Jiangsu Key Laboratory for Biosensors, Institute of Advanced Materials (IAM), Jiangsu National Synergetic Innovation Center for Advanced Materials (SICAM), Nanjing University of Posts & Telecommunications, 9 Wenyuan Road, Nanjing 210023, China

[†] These authors contributed equally to this article.

ABSTRACT

Rational molecular design leads to the achievement of β -conformations of terfluorenes that are usually difficult for oligoalkylfluorenes with less than 5 repeat units. Herein, under the guideline of synergistically molecular attractor-repulsor theory (SMART), we design four models of terfluorenes with the possibility of having the β -conformations in the terfluorene, 2,2'-(spiro[fluorene-9,9'-xanthene]-2,7-diyl) bis(9-(4-(octyloxy)phenyl)-fluorene-9-yl) (2O8-DPFOH-SFX) through manipulating the cooperative effect of steric hindrance, hydrogen bonding (HB) and van der Waals (vdW) force after thermal annealing. For terfluorene 2O8-DPFOH-SFX, the two isomers, raceme and mesomer, with two side chains residing on the two sides and the same side of fluorene backbone, respectively, have different packing styles and hence different optical properties: only the raceme isomer could induce the formation of β -conformation. Due to the steric pairing effect of side chains on both sides, and the cooperative interaction of middle spiro[fluorene-9,9'-xanthene] (SFX) group, racemes artfully interlace with each other and tend to adopt Δ -shaped stacking, which is more favorable for raceme to display planar π -conjugated structure. This is rationalized by the larger content of planar conformations in raceme of 2O8-DPFOH-SFX according to molecular dynamics (MD) simulations of the condensed phase. Oligofluorenes with definite molecular structure are considered as notable materials to gain insight into the structure-property relationships with the potential optical and electronic applications on demanding.

INTRODUCTION

Conformational transition has a significant influence on the physical and chemical properties of organic molecules, such as reversible switching, the origin of the glass transition temperature, plastic crystals, pharmaceutical polymorphs, specific phase and high performance. As one crucial but subtle item in organic and polymer semiconductors, conformation transition sometimes has the positive effect on electronic property or exciton that not only for electrical switching but also for the mobility and high efficiency, but sometimes disturbs the material functions and behaviors as defects.

Great efforts have been made to study conformation transition experimentally and theoretically from the aspects of statistical thermodynamic, kinetics and quantum mechanism. From the microscopic view of single molecular state, it has been recognized that the prerequisite to achieve the transition is to overcome the energy barrier between local minima. In terms of macroscopic thermodynamic theory, the occurrence of a transition process requires a negative value of the Gibbs free energy change (ΔG), which is the resultant from both enthalpy and entropy contributions. Indeed, from the kinetics standing point, not all the polyfluorenes could trigger the conformation transition even when heated to a high enough temperature.

Planar chain conformation, also called β -conformation in polyfluorenes, becomes a unique model to investigate the picture of molecular phase change.¹⁻¹⁹ The formation of β -conformation is usually characterized by the appearance of shoulder peak at around 430 nm in UV-*vis* absorption spectra and red-shifted emission peak at about 447 nm.^{20,21} To date, planar conformation has been studied intensively in consideration of both the inherently molecular design and external condition regulation. On the one hand, many efforts have been made to investigate the effects of molecular structure²², such as molecular weight^{23,24}, alkyl substituent,^{1,11} and copolymerization⁹, on the formation of β -conformation in polyfluorenes. On the other hand, one resorted to some convenient strategies focused on external environment regulation, including solubility in certain solvent²², solvation temperature variation²⁵, thermal annealing¹⁸, blending²⁶ and so on. Numerous progresses have been reported,

yet a few questions still exist, including the roles of the molecular segments; the thickness effects on β -conformation; the reason why some polyfluorenes with β -conformation while others without; the ways to incorporate between molecular structures and external conditions, and the difference between solvent crystallization induced β -conformation and thermal induced process. What's more, how to realize the electrically induced crystallization and phase change has become one thorny issue in optoelectronic semiconducting memory field.

Therefore, the state-of-the-art model is particularly important to understand the single-element node to map the whole picture. According to the attractor-repulsor molecular design,²⁷⁻³¹ Xie and coworkers sophisticatedly tuned the positions of bulky groups with steric hindrance and alkoxy side chains with vdW forces, and unprecedentedly obtained the β -conformation in a bulky polydiarylfuorene (PODPF).³² Except for polyfluorene, β -conformation has also been observed in some oligofluorenes. Oligofluorenes with well-defined chain lengths and definite molecular structure are considered as notable materials for understanding the structure-property relationship, in sharp contrast to polyfluorenes which have difficulty in precise characterization due to polydispersity and conformation complexity. Nakashina et al. reported that at least 15 or more repeating fluorene units are necessary to form β -conformation structure in oligo(9-9'-dioctylfluorenes).¹³ Moreover, the β -conformation of shorter main-chain oligomeric fluorene consisted of 5 monomer units was achieved by Lidzey et al.⁸ Recently, diarylfuorene dimers exhibit conformational planarization with a torsion angle of 180° , indicating the ability of very short oligofluorenes forming coplanar conformation.³³ We hence wonder that with the cooperative effects of the hydroxyl group (acting as the HB donor/acceptor), bulky spirofluorene group (with steric hinderance), and octyl side-chains (with favorable vdW forces) to tune the inter-chain arrangement, *is it possible to achieve planar backbone of short oligofluorenes in film or solution with proper chemical modification?*

In fact, planar conformation is the metastable state with the nature of the pervasive high-energy conformations, but can be stabilized by intermolecular

non-covalent interactions in some cases. Secondary interactions, such as van der Waals force, π - π interaction and hydrogen bonding interaction, have been proposed as a promising tool to modulate possible planarization when they are rationally incorporated into a molecular design. In this work, we attempted to achieve β -conformation in the fluorene trimer through the collective effects of HB interaction, bulky steric hindrance, and steric pairing effects of side chains. Herein, four terfluorenes were designed and synthesized: 2,2'-(spiro[fluorene-9,9'-xanthene]-2,7-diyl)bis(9-(4-(octyloxy)phenyl)-fluorene-9-ol) (2O8-DPFOH-SFX), 2,2'-(spiro[fluorene-9,9'-xanthene]-2,7-diyl)bis(9-phenyl-fluorene-9-ol) (DPFOH-SFX), 9,9''-bis(4-(octyloxy)phenyl)-9'-phenyl-[2,2':7',2''-terfluorene]-9,9',9''-triol (2O8-TPFOH) and 9,9',9''-triphenyl-[2,2':7',2''-terfluorene]-9,9',9''-triol (TPFOH). Unexpectedly, 2O8-DPFOH-SFX displays planar conformation after thermal annealing. An in-depth research reveals that 2O8-DPFOH-SFX exhibits the isomer-dependent conformation transition behavior and only the raceme-isomer favors the formation of β -conformation through the steric pairing effects between steric hindrance SFX group and two side chains on both sides. The molecular level insight into the origin of isomer-dependence formation of β -conformation and the HB promoted π stacking modes will be gained by the joint efforts of molecular dynamics (MD) simulations on packing structures, density functional theory (DFT) calculations on electronic structures, and NMR experiments of chemical shifts. The observation of β -conformation in short backbone-chain of oligofluorene and the insight into their packing modes provides a new opportunity for preparing novel systems and regulating the high electron transport properties in oligofluorene materials.

2. DETAILS of EXPERIMENTS AND COMPUTATIONS

2.1 Experimental Details

2.1.1 Chemicals

All the solvents and reagents were purchased from commercial suppliers and used without further purification unless otherwise noted. All products were purified by flash column chromatography using Kanto Silica Gel (Kanto Chemical Co., Inc., Xuhui District, Shanghai, China) 60N (40–63 μm). Spectrochemical-grade solvents were used for optical measurements. Palladium(II) acetate, tetra(triphenylphosphine)palladium, 1,1'-bis(diphenylphosphino)ferrocene (dppf), 2,7-dibromo-9-fluorenone, 2-bromo-9-fluorenone, bromobenzene, 1-bromo-4-(octyloxy) benzene, and 2,2'-bithiophene were obtained from Aldrich Chemical Co. (Xuhui District, Shanghai, China). Borontrifluorideetherate, potassium carbonate, magnesium sulfate, chloroform and toluene were purchased from Sinopharm Chemical Reagent Co, Ltd (Nanjing, Jiangsu, China) and were used without further purification. Dichloromethane was dried using anhydrous sodium at room temperature. THF and toluene were dried over the sodium using benzophenone as indicator and distilled under dry nitrogen atmosphere immediately prior to use. The following 2,7-dibromo-spiro[fluorene-9,9'-xanthene] (DBrSFX), 2,7-dibromo-9-phenyl-fluorene-9-ol (DBrPFOH), 2-bromo-9-phenyl-fluorene-9-ol (BrPFOH), 9-(4-(octyloxy)phenyl)-2-(4,4,5,5-tetramethyl-1,3,2-dioxaborolan-2-yl)-fluorene-9-ol (TMB-PFOHO8) and 2-(4,4,5,5-tetramethyl-1,3,2-dioxaborolan-2-yl)-9-phenyl-fluorene-9-ol (TMB-PFOH) were obtained according to previously published protocols.^{2,34-36}

2.1.2 Characterization

The ^1H and ^{13}C -NMR spectra were recorded in CDCl_3 with tetramethylsilane (TMS) as the internal standard reference, using a Bruker 400 MHz spectrometer. The mass spectra were recorded on a Shimadzu GC-MS 2010 PLUS. The MALDI-TOF MS spectra were recorded in the reflective mode using substrates. The absorption spectra

were measured using a Shimadzu UV-3600 spectrometer (Shimadzu Corporation, Nanjing, Jiangsu, China) at room temperature of the pristine films before and after annealing at 220 °C, and the emission spectra were recorded using a Shimadzu RF-530XPC luminescence spectrometer (Shimadzu Corporation, Nanjing, Jiangsu, China) after excitation at the absorption maxima. The thin films were prepared by spin-coating on a quartz plate at spin-coating speed of 1500 rpm from 10 mg/mL in toluene solution.

2.1.3. Synthesis of 2O8-DPFOH-SFX, DPFOH-SFX, 2O8-TPFOH and TPFOH via Suzuki Coupling Reaction

The fluorene tertiary alcohol monomer was synthesized via a Grignard reaction as previously reported.³⁵ The synthetic routes for 2O8-DPFOH-SFX, DPFOH-SFX, 2O8-TPFOH and TPFOH are shown in Figure S1.³⁶ The target oligofluorenols were synthesized via a palladium-catalyzed carbon-carbon Suzuki cross-coupling reaction. A typical preparation procedure is that under N₂ atmosphere, the reactants were added to a three-necked Schlenk flask (150 mL). The flask was evacuated and back-filled with nitrogen atmosphere more than three times before injecting with degassed toluene/THF (30 mL, 1:1 v/v) and an aqueous K₂CO₃ solution (5 mL, 10 eq) through a syringe. The reactant mixture was heated to 90 °C and stirred for 48 h. The mixture was poured into water and extracted with dichloromethane. The combined extracts were dried by anhydrous MgSO₄, and then the solvent was removed under vacuum condition. The product was purified by silica gel chromatography to afford powder product. The detailed information for synthetic routes was shown in Figures S1. ¹H, ¹³C-NMR, MALDI-TOF-MS, UV-*vis* absorption, photoluminescence spectrum, TLC photographs of 2O8-DPFOH-SFX, and MALDI-TOF-MS spectra of two isomers of 2O8-DPFOH-SFX were shown in Figures S2-S7. The calculated ¹H-NMR spectra were also given in Figures S4a.

2. 2 COMPUTATIONAL DETAILS

Molecular Dynamics Simulations. To study the packing structures of fluorenols (TPFOH, 2O8-TPFOH, DPFOH-SFX, 2O8-DPFOH-SFX) in amorphous state, several MD simulations were carried out in the canonical (NVT) ensemble at 298 K and the annealing at 493 K, respectively, by using Andersen thermostat.³⁷ The heating or cooling process in annealing was carried out by gradually raising or lowering the temperature 50 °C in each MD simulation, as illustrated by Figure S9 of SI. At each temperature, a 300 ps MD simulation was implemented to reach the equilibrium for the studied systems. In the last temperature raising step, the system was heated from 448 K by 45 °C to 493 K, which is the same condition used in experiments. After 300 ps MD simulation for reaching equilibrium, the cooling process was carried out according to the inverse process of the heating process (Figure S9). When temperature was cooled to 298 K, the 10-ns-MD simulation was subsequently carried out. The polymer consistent force field (PCFF)³⁸⁻⁴¹ is employed in this work to describe the packing structures of substituted and unsubstituted oligofluorenols in amorphous states. The performance of PCFF has been tested in our previous works of π -conjugated five-membered heterocyclic oligomers systems in amorphous phase.⁴²⁻⁴³ For the homologue of our studied TPFOH system, R-TFOH with one OC₈H₁₇ side-chain at 9-position of the middle of fluorenol unit was designed, PCFF was validated to be effective by quantum chemical calculations.⁴⁴ It would be useful to compare the PCFF optimized geometry with the crystal structure of the studied terfluorene. Unfortunately, we couldn't obtain suitable single crystals of terfluorene for single crystal X-ray diffraction after many trials via solvent diffusion method with different mixed solvent systems (such as dichloromethane/ethanol, tetrahydrofuran/isopropanol and chloroform/hexane systems et al.). Instead, the crystal structures of *cis/trans* DFOH (being substituted with OH group) and BSFX (with SFX group) were studied by using PCFF. Detailed results are shown in Table S1. One can find that PCFF can reproduce the experimental crystal structures of the selected fluorene oligomers.

To model amorphous solids, 20 oligofluorenols have been randomly distributed

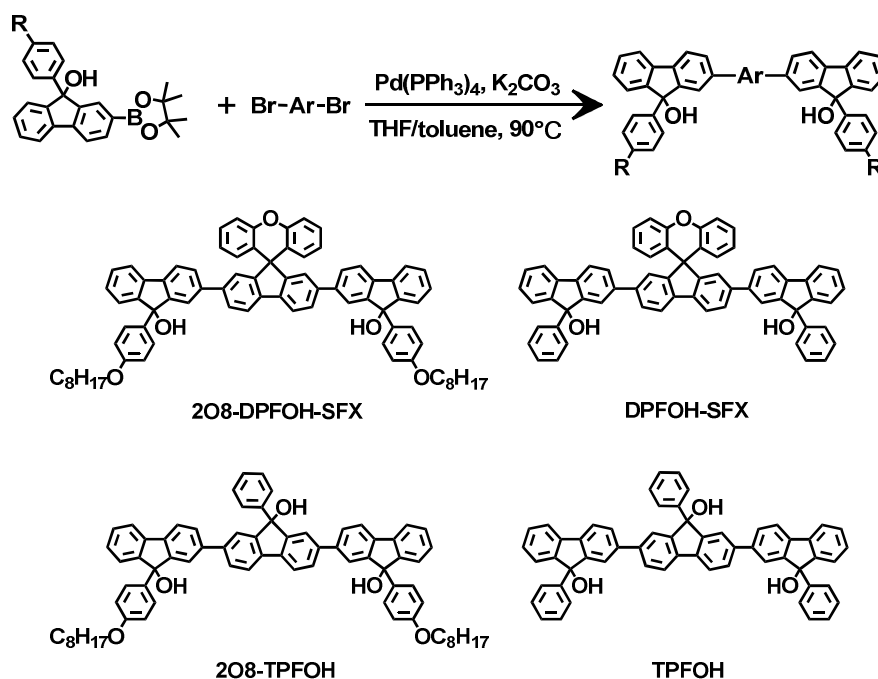
in the box with periodic boundary condition (PBC). The density, ρ , of amorphous is set to 1.03 g/cm^3 , which is close to experimental density of glassy α phase of PFO films ($\sim 1.04 \text{ g/cm}^3$).⁵ In order to gain a reasonable prediction of packing structures, some independent MD simulations were run with various different initial conformations. The cutoff of van der Waals interactions was set to be 15.5 \AA . The electrostatic interaction was evaluated by the Ewald summation. Motion equations were integrated by using the velocity Verlet algorithm with the time step of 1 fs. The 10-ns simulation was subsequently carried out after the equilibrium state has been reached at 298 K. We sampled the conformations from 10-ns-trajectories after annealing at 493 K for the subsequent absorption spectra calculations. All MD simulations were performed with the discover module in Materials Studio package.⁴⁵

Geometry and Vertical Excitation Energy. All DFT, vertical excitation energies and $^1\text{H-NMR}$ signals were performed using the Gaussian 09 program package.⁴⁶ The influence of various DFT functionals including BLYP, PBE, B3LYP, CAM-B3LYP, wB97XD, and M06-2X, on the maximum absorption peak, λ_{max} , have been tested for fluoreneol monomer MFOH, DFOH with two fluoreneol units, R-PFOH with three fluoreneol units and one octyloxy side-chain at the middle of the fluoreneol unit at 9-position,⁴⁴ as well as other π -conjugated systems⁴⁷. Accordingly, the theoretical level of CAM-B3LYP and 6-31+G(d) basis set was selected to calculate the absorption spectra and $^1\text{H-NMR}$ signals in this work. The ground state geometries of terfluorenes were optimized using the B3LYP functional and 6-31+G(d) basis set for all the C, H, and O atoms. The self-consistent field (SCF) convergence criteria for geometry optimization and vertical excited energy and $^1\text{H-NMR}$ signals were set to 10^{-6} a.u. The DFT-based $^1\text{H-NMR}$ chemical shifts (δ) were computed by using gauge invariant atomic orbital (GIAO) method.

3. RESULTS AND DISCUSSION

3.1 Synthesis and Optical Properties of Four Terfluorenes

In order to achieve conformation transition of terfluorenes by supramolecular steric hindrance (SSH) principle, we designed and synthesized the model terfluorene, 2O8-DPFOH-SFX that contains SFX as bulky groups with repulsion force, hydroxyls with hydrogen bonding interaction and alkoxy chains with vdW force. We also synthesized model molecules named DPFOH-SFX without alkoxy side chains at the phenylfluorenes, 2O8-TPFOH without SFX core and TPFOH for comparison to carefully clarify the exact roles of each segment (Scheme 1). The synthetic routes of intermediates and terfluorenes are shown in Figure S1. The terfluorenes display the high decomposition temperatures (T_d) of 340, 379, 272, 330 °C for 2O8-DPFOH-SFX, DPFOH-SFX, 2O8-TPFOH and TPFOH (Figure S8), respectively, indicating that the four terfluorenes have high thermal stability.



Scheme 1. The synthetic route and chemical structures of 2O8-DPFOH-SFX, DPFOH-SFX, 2O8-TPFOH, and TPFOH.

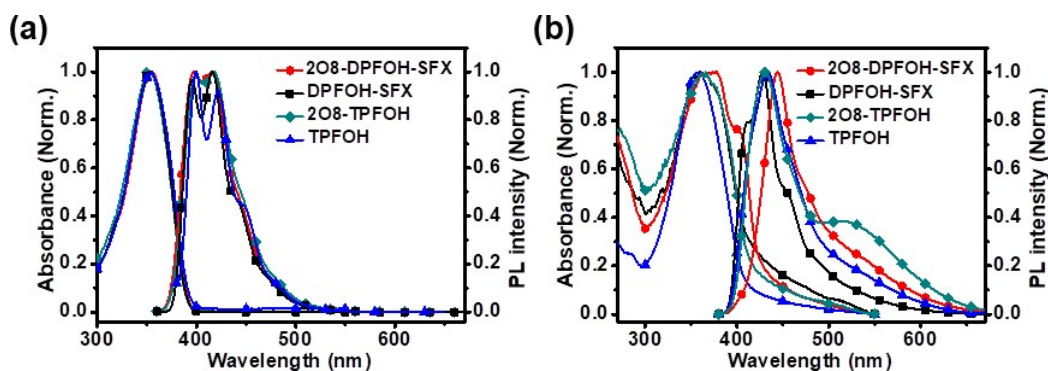


Figure 1. Optical properties of the synthesized terfluorenes. The experimental UV-*vis* absorption and photoluminescence spectra of (a) toluene dilute solution and (b) films spin-coated from toluene solution after thermal annealing at 220 °C in N₂ environments.

The photophysical properties of terfluorenes in solution and film states are shown in Figures 1 and S5. All the terfluorenes show only one absorption band in both solution and spin-coated film. The maximum absorption peaks are at 354 nm in dilute solution attributed to main-chain backbones of oligofluorenes, and only show a red-shift with ~3 nm in solid films (Figure 1a and S5a). The emission spectra of four terfluorenes exhibit three similar well-resolved emission bands at 396, 416, 442 nm, corresponding to 0-0, 0-1, and 0-2 vibronic transitions, respectively, and show a slight difference in solution. In terms of films, the PL spectra show the similar emission behavior (Figure S5b). Above results indicate that the alkoxy and bulky substituents have a little influence on the electronic structures of terfluorene backbones. Interestingly, 2O8-DPFOH-SFX exhibited dramatic differences in absorption and emission spectra of films after annealing process compared to other molecules (Figure 1b). Apart from the maximum absorption peak at 364 nm, the appearance of the shoulder peak at 402 nm, which was similar to the characteristic absorption peak of PFO β -conformation at 436 nm,^{20,21} confirms the formation of β -conformation. Moreover, the red-shifted PL spectrum about 16 nm further supports this point. While DPFOH-SFX and 2O8-TPFOH only showed a red-shift of 5 nm in absorption spectra with the absence of shoulder peak. It is worth noting that, with the introduction of two octyloxy

side-chains and absence of SFX group in 2O8-TPFOH, there was a broad peak at 500-600 nm (green band emission) in the photoluminescence spectra.

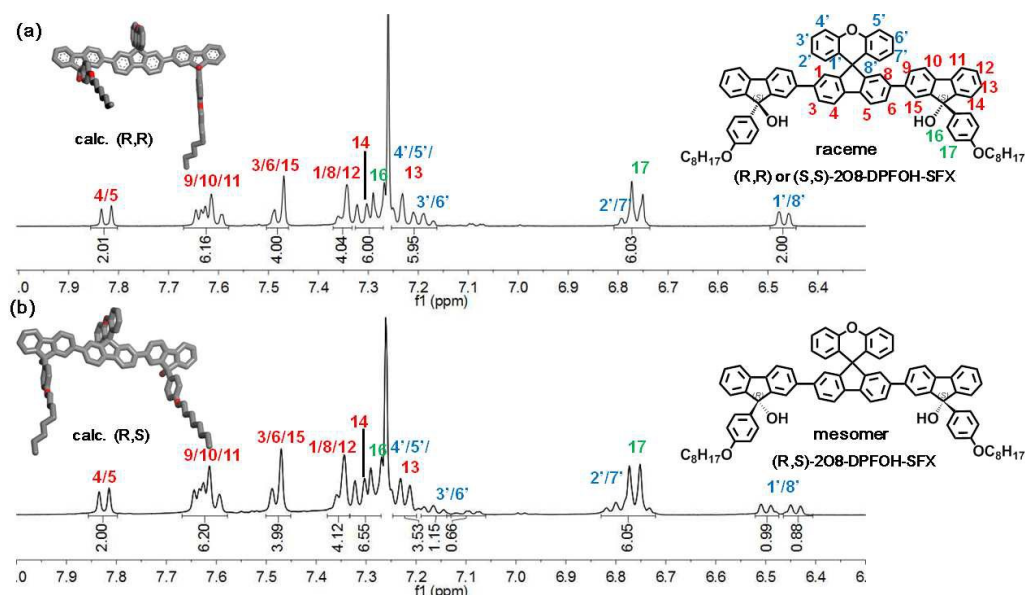


Figure 2. ^1H NMR spectra of two isomers of 2O8-DPFOH-SFX with different molarity in CDCl_3 , (a) two side chains at the different sides, namely raceme including (R,R) or (S,S)-configurations; (b) two side chains at the same side, namely mesomer including (R,S) –configuration. The DFT optimized (calc.) geometries of two isomers are also presented.

During the separation and purification process, surprisingly, two isomers of 2O8-DPFOH-SFX were observed in TLC and confirmed via ^1H NMR. As seen in Figure S6, owing to the polarity difference, spots of the two isomers can be observed from TLC under 254 nm UV lamp. We purified the isomers separately, and determined their molecular weight of 1099.5 by the MALDI-TOF-MS spectra (Figure S7). Theoretical calculations indicate that the ground state energy of raceme with the side chain groups lying at the different sides is close to that mesomer with the energy difference of less than 2 kcal/mol, supporting the concurrence of two isomers in experiment. As shown in Figure 2, the two isomers show the similar ^1H NMR spectra, and the most notable peak is at 1' and 8' position of the spiro[fluorene-9,9'-xanthene]. As for the hydroxyl groups at the same side, the chemical shifts of xanthene are

nonequivalent, leading to the split signals shown in Figure 2. The calculated NMR spectra of two different isomers are in good agreement with experiments (Figure S4a). The optimized structures and relative energies of the different isomers were presented in Table S2.

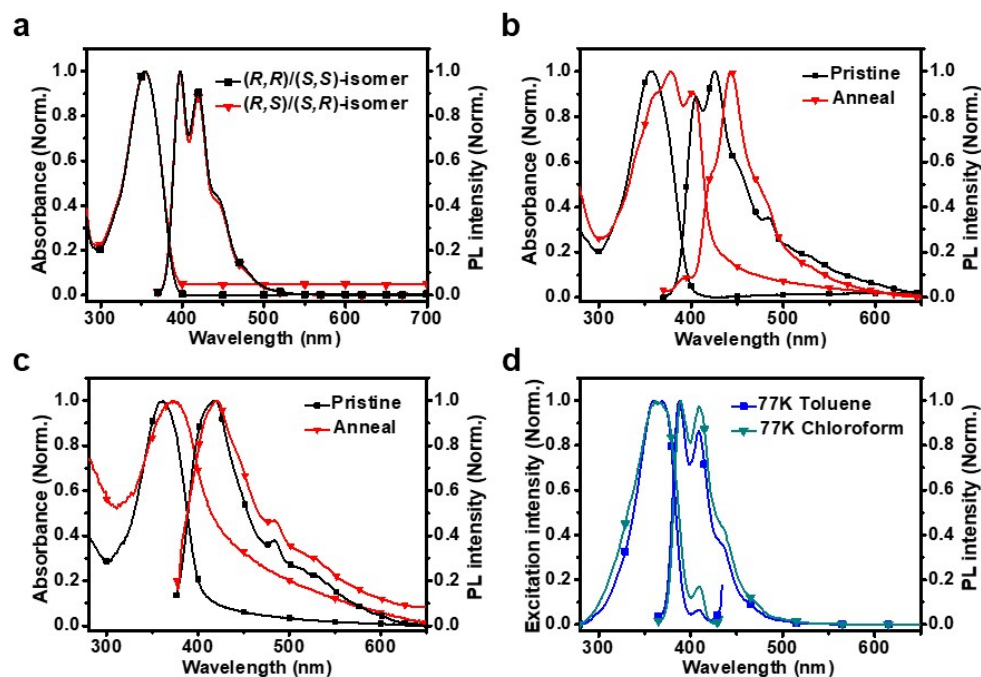


Figure 3. (a) The experimental UV-*vis* absorption and photoluminescence spectra of isomers in toluene dilute solution. (b) Absorption and emission spectra of raceme of 208-DPFOH-SFX films before and after thermal treatment under 220 °C in N₂. (c) Absorption and emission spectra of mesomer of 208-DPFOH-SFX films before and after thermal treatment under 220 °C in N₂. (d) PL and excitation spectra of raceme of 208-DPFOH-SFX in dilute toluene and CHCl₃ solutions (10⁻³ mg/mL) at low temperature ambient (liquid nitrogen), respectively.

The photophysical properties of isomers in solution and film states are shown in Figure 3. Both the isomers have only one absorption band at 355 nm and three well-resolved emission bands at 397, 419 and 444 nm in dilute solution (Figure 3a). Interestingly, the two isomers of 208-DPFOH-SFX exhibit dramatic differences in absorption and emission spectra of spin-coated films after thermal treatment. For the

pristine raceme of 2O8-DPFOH-SFX film, the maximum peak is observed at 358 nm for UV-*vis* spectra, and the corresponding PL spectra consisted of four emission bands at 405, 425, 452 and 484 nm in Figure 3b. And for the mesomer, the maximum absorption peak appears at 360 nm, and PL spectra consisted of two emission bands at 418 and 484 nm in Figure 3c. However, dramatic differences appeared after thermal annealing. Besides the 360 nm main peak, a shoulder peak at 402 nm in Figure 3b was found in the UV-*vis* spectra of raceme-terfluorene, indicating the existence of planar conformation. Moreover, the obvious red-shifts occur in the PL spectrum of raceme-terfluorene. In addition, the fluorescence quantum efficiency of planar conformation (54%) is lower than amorphous state (66%). But for the mesomer-terfluorene, the maximum absorption peak in Figure 3c is bathochromic 13 nm from 360 nm to 373 nm without the appearance of shoulder peak after annealing process, reflecting that this isomer only has the trend of crystalline but not of planarity. To the best of our knowledge, the isomer-dependent conformation transition in short-backbone chain terfluorene has never been reported in previous literatures.

In order to probe whether β -conformation of raceme-terfluorene could be generated in dilute solution, low-temperature optical analysis was employed here (Figure 3d). The appearance of the shoulder peaks at 409 nm at liquid nitrogen ambient confirms the formation of planar conformation in dilute toluene and CHCl_3 solid solution (solvents show solid state at such low temperature). PL spectra of raceme of 2O8-DPFOH-SFX in dilute solid solution exhibited three well-resolved emission bands at 388, 409, and 436 nm, respectively, and no red-shifts happened (Figure 3d). In our previous work, the content of the β -conformation was not sufficient to realize completely energy transfer from amorphous state to β -conformation. Here, this β -conformation emission needed more content of planar chains compared with PFO (~1% for PFO), which can be ascribed to a lower efficiency of energy transfer. The low-temperature induced conformation transition might be the result of molecular aggregation and lower molecular rotation. At 77 K, inter-chain interactions are maximized and sufficient to overcome the steric repulsion, and finally facilitated the conformation planarization.¹ The gaseous structure of raceme is slightly energetically

lower than the mesomer-structure, as predicted at both B3LYP/6-31+G(d) and PCFF levels (Table S2 of SI). The optimized packing structures of 20 chains in a cubic box with the periodic boundary condition show that the packed raceme solid has larger amount of planar segments than that in mesomer one, correlating with the appearance of shoulder peak at ~ 402 nm in UV-*vis* absorption spectra.

The simulated packing structures of isomers, raceme and mesomer, of 2O8-DPFOH-SFX in amorphous state are schematically shown in Figure 4. For raceme the two side chains were on both sides of fluorene backbone, leading to the evenly aligned Δ -shaped stacking with the inter-chain distance of about 12-14 Å in each side of a triangle (called ‘ Δ ’ here). However, for mesomer, whose side chains were on the same side of fluorene backbone, the two neighboring backbones are bundled together in an X-shape with a smaller inter-chain distance of about 9 Å. Such an interlace arrangement was also called steric pairing effect in previous works done by Yao and coworkers^[48,49]. The steric pairing effects in Δ -shaped stacking of raceme led to the increase of planar conformations. In contrast, the X-shaped stacking mesomers formed some unevenly distributed clusters in aggregate with their side chains stretching outside, just like pine needles.

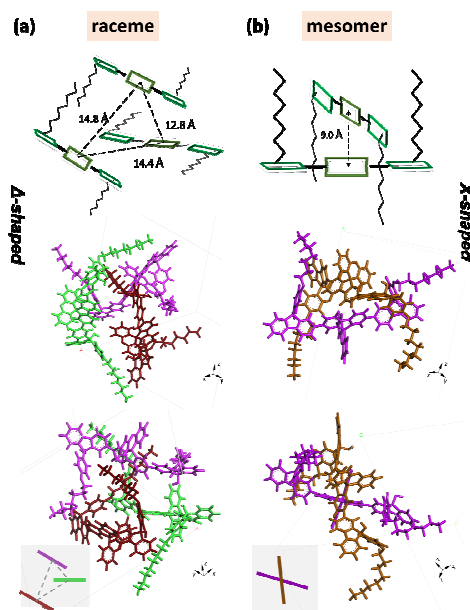


Figure 4. Schematic structure and representative packing pattern of the amorphous state of the (a) raceme and (b) mesomer of 2O8-DPFOH-SFX system. The other

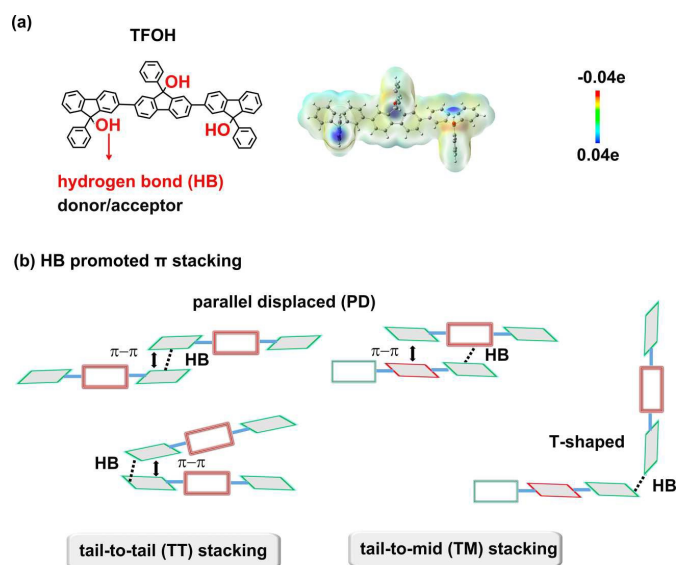
chains are not shown for clarity.

3.2 Theoretical Study on Packing Structures and Optical Properties of Four Terfluorenes

In order to give a deeper understanding on the role of SFX and side-chain groups played in photophysics properties and the origin of the appearance of β -phase in the 2O8-DPFOH-SFX, we further made the joint efforts of molecular dynamics (MD) simulations on packing structures and density functional theory calculations on electronic structures. The molecular level insight would be gained in the aggregation effects on the optical properties in the condensed phase.

3.2.1 Molecular Aggregation and the Effect of HB Interaction on the $^1\text{H-NMR}$.

The existence of intermolecular hydrogen bonding (HB) interaction between the adjacent TPFOH molecules significantly affects the aggregation modes. In fact, the self-assemble behavior of H-bond donor and acceptor sites has been utilized to regulate the fold and duplex via intra- or intermolecular H-bonds of oligomers.⁵⁰ It was also found in zinc porphyrin–pyridine ligand complexes that the formation of intramolecular H-bonding interactions enabled the evaluation of the effect of conformational flexibility on cooperativity in supramolecular complexes.⁵¹ As shown in Scheme 2, there are two kinds of stacking modes, tail-to-tail (TT) and tail-to-mid (TM), named as the relative position of anchor sites (i.e., hydroxyl groups in the terminal and middle units) for HB interactions. For a trimeric system, the number of hydroxyl groups in terminal units is twice that in the center group. It can be thus anticipated that the TT stacking, with the HB formed between two terminal groups, is more popular than the TM packing style. In the TT stacking, the conjugated segments in two different chains are usually parallel displaced (PD) stacked. Different from TT stacking, TM stacking mainly adopted two modes, parallel displaced (PD) and T-shaped stacking, depending on the relative orientation of two neighboring TPFOH chains.



Scheme 2. Effects of hydrogen bonding on packing modes of oligofluorens.

Figure 5 depicts the difference in packing structures caused by the addition of side chains or steric SFX group. Without chemical modification, unsubstituted TPFOH mainly adopted TT packing with the percentage of about 85%. The typical snapshot selected from MD simulation shows the all-twist structure in TPFOH backbone. The introduction of OC_8H_{17} side-chains in the terminal unit seems to cut down the superiority of TT stacking and leads to a balanced distribution of two packing modes in 2O8-TPFOH with 51% TT and 49% TM stacking. The planar segments appeared in the selected snapshots, probably contributing to the broad peak at 500-600 nm (green band emission) in the photoluminescence spectra of 2O8-TPFOH (Figure 1). The side-chain effect can be also reflected by the intermolecular distance, which was measured by the distance between the centroids of two fluorene units of adjacent TPFOH molecules. The addition of the OC_8H_{17} long side-chain in 2O8-TPFOH increases the intermolecular distance to 6 Å, which is longer than that (5 Å) in TPFOH and DPFOH-SFX. The stacking distances in TPFOH, DPFOH-SFX and 2O8-TPFOH oligomers were longer than that (3.7 Å) reported for poly(9,9'-dioctylfluorene), but shorter than that (7.3 Å) that reported in 2,7-PFs in amorphous states⁵² and that (11.8 Å) of *cis* DFOH crystal in our previous work.⁴⁴ For both DPFOH-SFX and 2O8-DPFOH-SFX, the replacement of SFX group in the

middle unit does not alter much the predominance of TT aggregation modes in comparison with TPFOH. However, the planarity is enhanced and the percentage of twist-planar or all-planar conformations is increased in 2O8-DPFOH-SFX.

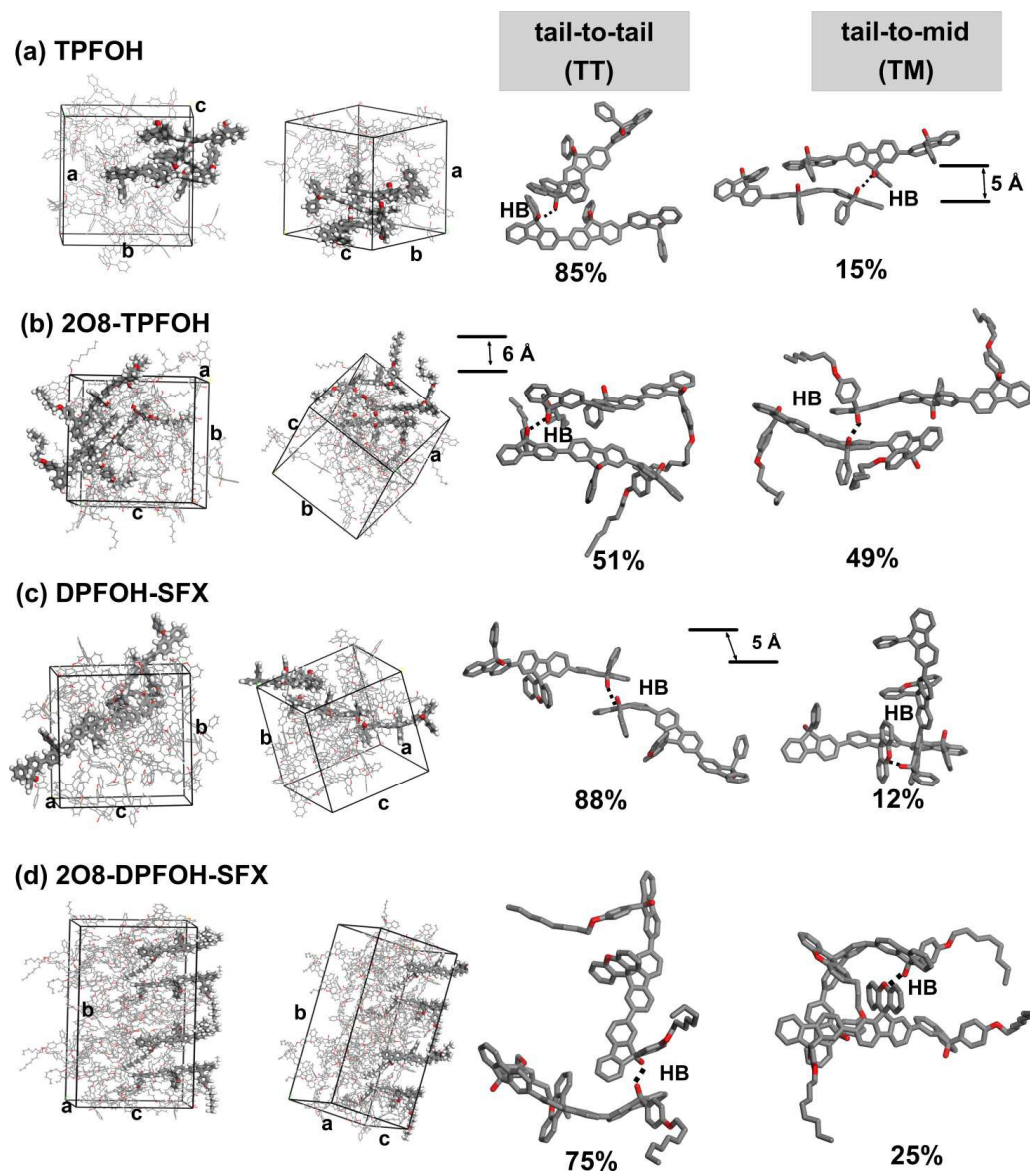


Figure 5. Representative snapshots and packing pattern of the MD-simulated amorphous of substituted and unsubstituted TPFOH type systems. In amorphous phase, 20 oligofluorenols have been initially randomly distributed in the PBC box. The density of oligofluorenols is set to 1.03 g/cm^3 , which is close to experimental density of glassy α phase of PFO films ($\sim 1.04 \text{ g/cm}^3$).⁵ the sizes of simulation cells were $2.9 \times 2.9 \times 2.9 \text{ nm}^3$ for (a) TPFOH, $3.2 \times 3.2 \times 3.2 \text{ nm}^3$ for (b) 2O8-TPFOH, $3.0 \times 3.0 \times 3.0 \text{ nm}^3$ for (c) DPFOH-SFX, $3.3 \times 3.3 \times 6.6 \text{ nm}^3$ for (d) 2O8-DPFOH-SFX.

The formation of intermolecular HB can be reflected in the change of $^1\text{H-NMR}$ from the isolated TPFOH molecule to the molecular aggregates. Shown in Figure S10 are the calculated NMR spectra of isolated molecule and a pair of stacked molecules, along with the experimental spectra for comparison. It clearly indicated that the chemical shift of H proton of hydroxyl groups in TPFOH aggregates downshifted obviously, relative to that predicted for an isolated molecule at the same theoretical level. The calculated $^1\text{H-NMR}$ spectra of oligofluorenol aggregates are consistent with the experimental results.

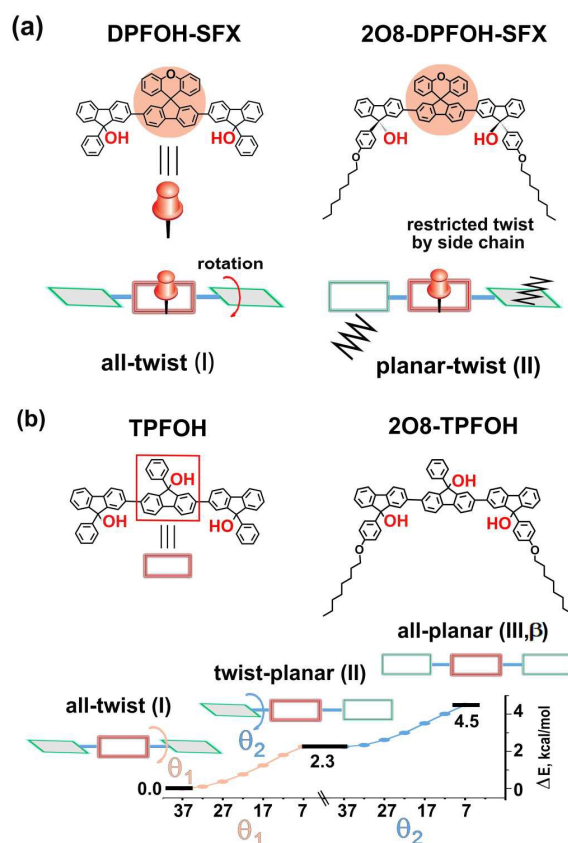
3.2.2 β -Phase: UV-vis Absorption and Emission Spectra

Chemical modification of TPFOH not only affects their molecular packing but also allows the appearance of various conformations, which may be energetically unfavorable in vacuum. For an isolated molecule, there is little difference in gaseous geometry of backbone and rotation barrier of inter-unit bond caused by the introduction of side-chain or/and SFX group in TPFOH (Figure S11). The torsion angles between adjacent fluorenol units of the studied TPFOH family were around 35° - 39° . Such highly twisted backbones were planarized to some extent in amorphous state or film due to aggregation. Compared with the isolated molecule in vacuum, the torsion angles of both substituted and unsubstituted TPFOH in amorphous distributed in a very broad range including some small torsion angles of less than 15° , indicating the presence of planar conformations. The percentage of planar conformations, $\beta\%$, is analyzed with the criterion of $D1 < 15^\circ$ and $D2 < 15^\circ$ ($D1$ and $D2$ was the torsion angle between two adjacent fluorenol units as shown in Figure S11) in trimeric fluorenols. In the molecular aggregates, the content of β -phase of 2O8-DPFOH-SFX was 0.42%, higher than that (0.076%) in DPFOH-SFX and (0.13%) in 2O8-TPFOH. The maximum absorption peaks of four typical planar conformations (which were sampled from MD trajectories) were red-shifted to about 415-469 nm relative to that (324-328 nm) predicted in vacuum, as shown in Figure S12.

As discussed above, the simultaneous adding of side-chain and SFX group in 2O8-DPFOH-SFX brought out the most evident changes in the relative percentage of

various possible conformations. The 2O8-DPFOH-SFX was then selected to study the relationship between the three typical conformations (all-twist, twist-planar, all-planar) and UV-*vis* absorptions spectra in Figure S13. The planarity of all-planar conformation of 2O8-DPFOH-SFX renders the maximum absorption peak, λ_{\max} , in UV-*vis* absorption spectra red-shifted to 412 nm, in comparison with that λ_{\max} =370 nm for all-twist conformation and λ_{\max} =405 nm for the twist-planar one. The major orbital contributions for λ_{\max} of these three kinds of conformations were involved with the transition from the highest occupied molecular orbital (HOMO, called H for short) to the lowest unoccupied molecular orbital (LUMO, called L). For all-twist conformations the HOMO and LUMO are mainly located in two fluorene repeat units. But with the enhancement in planarity, the orbitals are delocalized in the whole fluorene backbone for twist-planar and all-planar conformations.

We further studied the calculated and experimental absorption spectra of substituted and unsubstituted TPFOH after annealing at 493 K. As shown in Figure S14, the calculated absorption spectra are in consistent with the experimental absorption spectra. The maximum absorption peak of TPFOH with two OC_8H_{17} side-chains (2O8-TPFOH) or with one SFX group (DPFOH-SFX) occurs to slight red-shift relative to that of unsubstituted oligomer TPFOH (TFOH: 360 nm; 2O8-TPFOH: 367 nm; DPFOH-SFX: 363 nm). The cooperative effect of two OC_8H_{17} side-chains and SFX group caused the absorption spectra of 2O8-DPFOH-SFX exhibiting a shoulder peak at ~405 nm, which was the characteristic peak of β -phase in PFs.^{20,21}



Scheme 3. Chemical modifications on oligofluorenols and their possible conformations.

As shown in Scheme 3, the transitions from the most favorable all-twist to the metastable twist-planar and all-planar conformations need to overcome rotation barriers of about 2.3 and 4.5 kcal/mol, respectively. The values were close to the energy (3.7 ± 0.6 kcal/mol) required to planarize the fluorene backbone reported by Monkman experimentally.¹ In the center of trimeric fluorenol, a spiro [fluorene-9,9'-xanthene] (SFX) group is introduced as a pin to fix the middle point of terfluorene. It is shown that with the steric pairing effect of two octyloxy side-chains on both sides and the cooperative interplay with SFX group in raceme of 2O8-DPFOH-SFX, the backbone torsion was largely restricted, resulting in the increase of planar segments in such a short chain.

4. CONCLUSIONS

In conclusion, we demonstrated the rational molecular design using the cooperative effect of hydrogen bonding, steric hindrance and van der Waals forces to achieve the β -phase in short-backbone chain terfluorene 2O8-DPFOH-SFX by thermal annealing. For the first time, we observed the isomer dependence of the β -phase conformation and only the raceme-isomer of 2O8-DPFOH-SFX could induce β -conformation. Theoretical calculations were further carried out to study the origin of isomer-dependence and the effect of octyloxy side chains, steric hindrance group, HB interaction on their stacking structure and intramolecular torsion. With the cooperation effect of steric hindrance group and supramolecular weak interaction, the content of planar fragments was greatly increased in 2O8-DPFOH-SFX. Molecular dynamics simulations revealed that the larger-content planar conformations in raceme-structures of 2O8-DPFOH-SFX make it induce β -conformation. With the cooperative steric interaction of the middle spirofluorene SFX, the octyloxy side-chains on different sides of 2O8-DPFOH-SFX backbone artfully manipulated the intramolecular structure and staggered well into Δ -like array to facilitate the appearance of planar conformations in raceme. Due to the steric pairing effect, mesomers, whose two side chains are on the same side of backbones, take X-shaped stacking into some unevenly distributed clusters, and the long side-chains in the two ends of 2O8-TPFOH resulted in two competitive packing models. Tail-to-tail (TT) and tail-to-mid (TM) through weakening the intermolecular hydrogen bonding between the terminal groups, are predominant in other oligomers. The obvious low-frequency shift of chemical shift of proton ^1H in $^1\text{H-NMR}$ spectrum of molecular aggregates relative to the isolated molecule indicated the presence of hydrogen bonding interaction in TPFOH and its derivatives. The modulation of packing structures through the tunable steric pairing and hydrogen bonding networks gives rise to a new strategy in rational design of novel materials with the desired optical and electronic properties.

ASSOCIATED CONTENT

Supporting Information Available: This material is available free of charge via the Internet. Experimental Section: preparation of thin films for optical analysis; synthesis of DPFOH-SFX, 2O8-TPFOH and 2O8-DPFOH-SFX, and their ^1H , ^{13}C -NMR and MALDI-TOF-MS; UV-*vis* absorption and photoluminescence spectrum; TLC photographs of 2O8-DPFOH-SFX; MALDI-TOF-MS spectra of two isomers of 2O8-DPFOH-SFX. Computational Section: the heating and cooling process in simulation annealing; the optimized ground state geometries, packing structures and relative energies of the different isomers of 2O8-DPFOH-SFX; the experimental and calculated ^1H -NMR and UV/Vis absorption spectra in vacuum and amorphous state; typical planar conformations and their populations according to 10 ns MD-simulation for four terfluorenes; The major molecular orbital contributions for λ_{max} in UV-*vis* absorption spectra of different conformations in 2O8-DPFOH-SFX; the coordination of optimized structures of 2O8-DPFOH-SFX isomers.

AUTHOR INFORMATION

Corresponding Authors

*(J. Ma) E-mail: majing@nju.edu.cn Tel: (86)25-89687408.

*(L. Xie) Email: iamlhxie@njupt.edu.cn

Notes

The authors declare no competing financial interest.

ACKNOWLEDGEMENTS

This work was supported by the National Natural Science Foundation of China (Grant Nos. 21290192, 21673111, U1301243, 21274064 and 21703118), the Priority Academic Program Development of Jiangsu Higher Education Institutions, PAPD (YX03002), the Six Peak Talents Foundation of Jiangsu Province (XCL-CXTD-009), Open Project from State Key Laboratory of Supramolecular Structure and Materials at Jilin University (sklssm201710), Shandong Provincial Natural Science Foundation, China (No.ZR2017MB038). Project was funded by the Priority Academic Program Development of Jiangsu Higher Education Institutions. We are grateful to the High Performance Computing Center of Nanjing University for doing the quantum

chemical calculations in this paper on its IBM Blade cluster system.

REFERENCES

- 1 D. W. Bright, F. B. Dias, F. Galbrecht, U. Scherf and A. P. Monkman, *Adv. Funct. Mater.*, 2009, **19**, 67-73.
- 2 U. Scherf and E. J. List, *Adv. Mater.*, 2002, **14**, 477-487.
- 3 I. Franco and S. Tretiak, *J. Am. Chem. Soc.*, 2004, **126**, 12130-12140.
- 4 S. H. Chen, A. C. Su and S. A. Chen, *J. Phys. Chem. B*, 2005, **109**, 10067-10072.
- 5 S. H. Chen, A. C. Su, C. H. Su and S. A. Chen, *Macromolecules*, 2005, **38**, 379-385.
- 6 E. Da Como, K. Becker, J. Feldmann and J. M. Lupton, *Nano lett.*, 2007, **7**, 2993-2998.
- 7 H. H. Lu, C. Y. Liu, C. H. Chang and S. A. Chen, *Adv. Mater.*, 2007, **19**, 2574-2579.
- 8 W. C. Tsoi, A. Charas, A. J. Cadby, G. Khalil, A. M. Adawi, A. Iraqi, B. Hunt, J. Morgado and D. G. Lidzey, *Adv. Funct. Mater.*, 2008, **18**, 600-606.
- 9 J. Peet, E. Brocker, Y. Xu and G. C. Bazan, *Adv. Mater.*, 2008, **20**, 1882-1885.
- 10 M. S. Mehata, C. S. Hsu, Y. P. Lee and N. Ohta, *J. Phys. Chem. C*, 2009, **113**, 11907-11915.
- 11 L. L. Justin, A. T. Marques, C. J. Kudla, U. Scherf, L. Almásy, H. D. Burrows and A. P. Monkman, *Macromolecules*, 2010, **44**, 334-343.
- 12 L. Huang, X. Huang, G. Sun, C. Gu, D. Lu and Y. Ma, *J. Phys. Chem. C*, 2012, **116**, 7993-7999.
- 13 T. Shiraki, S. Shindome, F. Toshimitsu, T. Fujigaya and N. Nakashima, *Polym. Chem.*, 2015, **6**, 5103-5109.
- 14 A. Perevedentsev, S. Aksel, K. Feldman, P. Smith, P. N. Stavrinou and D. D. Bradley, *J. Polym. Sci. Part B: Polym. Phys.*, 2015, **53**, 22-38.
- 15 F. P. D. Costa, A. L. Maçanita, J. Morgado, F. B. Dias, H. D. Burrows and A. P. Monkman, *Macromolecules*, 2006, **39**, 5854-5864.
- 16 D. D. C. Bradley, M. Grell, X. Long, H. Mellor, A. W. Grice, M. Inbasekaran and E. P. Woo, *Proc. SPIE*, 1977, **3145**, 254-259.
- 17 M. Grell, D. D. C. Bradley, X. Long, T. Chamberlain, M. Inbasekaran, E. P. Woo and M. Soliman, *Acta Polym.*, 1998, **49**, 439-444.
- 18 M. Grell, D. D. C. Bradley, G. Ungar, J. Hill and K. S. Whitehead, *Macromolecules*,

- 1999, **32**, 5810-5817.
- 19 L. Huang, L. Zhang, X. Huang, T. Li, B. Liu and D. Lu, *J. Phys. Chem. B*, 2014, **118**, 791-9.
- 20 P. E. Shaw, A. Ruseckas, J. Peet, G. C. Bazan and I. D. Samuel, *Adv. Funct. Mater.*, 2010, **20**, 155-161.
- 21 A. K. Bansal, A. Ruseckas, P. E. Shaw and I. D. Samuel, *J. Phys. Chem. C*, 2010, **114**, 17864-17867.
- 22 M. Knaapila and A. P. Monkman, *Adv. Mater.*, 2013, **25**, 1090-1108.
- 23 C. W. Cone, R. R. Cheng, D. E. Makarov and D. A. V. Bout, *J. Phys. Chem. B*, 2011, **115**, 12380-12385.
- 24 T. Li, B. Liu, H. Zhang, J. Ren, Z. Bai, X. Li, T. Ma and D. Lu, *Polymer*, 2016, **103**, 299-306.
- 25 A. L. T. Khan, P. Sreearunothai, L. M. Herz, M. J. Banach and A. Köhler, *Phys. Rev. B: Condens. Matter Mater. Phys.*, 2004, **69**, 085201.
- 26 M. Campoy-Quiles, T. Ferenczi, T. Agostinelli, P. G. Etchegoin, Y. Kim, T. D. Anthopoulos, P. N. Stavrinou, D. D. C. Bradley and J. Nelson, *Nature Mater.*, 2008, **7**, 158-164.
- 27 L. H. Xie, Y. Z. Chang, J. F. Gu, R. J. Sun, J. W. Li, X. H. Zhao and W. Huang, *Acta Phys. Chim. Sin.*, 2010, **26**, 1784-1794.
- 28 L. H. Xie, C. R. Yin, W. Y. Lai, Q. L. Fan and W. Huang, *Prog. Polym. Sci.*, 2012, **37**, 1192-1264.
- 29 L.-H. Xie, X.-Y. Hou, C. Tang, Y.-R. Hua, R.-J. Wang, R.-F. Chen, Q.-L. Fan, L.-H. Wang, W. Wei, B. Peng, and W. Huang. *Org. Lett.*, 2006, **8**, 1363-1366.
- 30 L.-H. Xie, X.-Y. Hou, Y.-R. Hua, Y.-Q. Huang, B.-M. Zhao, F. Liu, B. Peng, W. Wei and W. Huang, *Org. Lett.*, 2007, **9**, 1619-1622.
- 31 L.-H. Xie, R. Zhu, Y. Qian, R.-R. Liu, S.-F. Chen, J. Lin and W. Huang, *J. Phys. Chem. Lett.*, 2009, **1**, 272-276.
- 32 J. Y. Lin, W. S. Zhu, F. Liu, L. H. Xie, L. Zhang, R. Xia, G. C. Xing and W. Huang, *Macromolecules*, 2014, **47**, 1001-1007.
- 33 C. J. Ou, C. Zhu, X. H. Ding, L. Yang, J. Y. Lin, L.-H. Xie, Y. Qian, C.-X. Xu, J.-F.

- Zhao and Huang, *W. J. Mater. Chem. C*, 2017, DOI: 10.1039/C7TC00675F.
- 34 E. J. List,; R. Guentner,; P. Scanducci de Freitas and U. Scherf, *Adv. Mater.*, 2002, **14**, 374-378.
- 35 L. H. Xie, F. Liu, C. Tang, X. Y. Hou, Y. R. Hua, Q. L. Fan and W. Huang, *Org. Lett.*, 2006, **8**, 2787-2790.
- 36 G. W. Zhang, L. Wang, L. H. Xie, J. Y. Lin and W. Huang, *Int. J. Mol. Sci.*, 2013, **14**, 22368-22379.
- 37 H. C. Andersen, *J. Chem. Phys.*, 1980, **72**, 2384.
- 38 S. R. Marder, J. W. Perry, B. G. Tiemann, C. B. Gorman, S. Gilmour, S. Biddle and G. Bourhill, *J. Am. Chem. Soc.*, 1993, **115**, 2524-2526.
- 39 M. J. Hwang, T. P. Stockfisch and A. T. Hagler, *J. Am. Chem. Soc.*, 1994, **116**, 2515-2525.
- 40 H. Sun, *Macromolecules*, 1995, **28**, 701-712.
- 41 H. Sun, S. J. Mumby, J. R. Maple and A. T. Hagler, *J. Phys. Chem.*, 1995, **99**, 5873-5882.
- 42 G. Zhang, J. Ma and J. Wen, *J. Phys. Chem. B*, 2007, **111**, 11670-11679.
- 43 G. Zhang, Y. Pei, J. Ma, K. Yin and C.-L. Chen, *J. Phys. Chem. B*, 2004, **108**, 6988-6995.
- 44 X. Yuan, W. Zhang, L. H. Xie, J. Ma, W. Huang and W. Liu, *J. Phys. Chem. B*, 2015, **119**, 10316-10333.
- 45 Materials studio, Version 4.0; Accelrys, Inc.: San Diego, 2006.
- 46 M. J. Frisch, G. W. Trucks, H. B. Schlegel, G. E. Scuseria, M. A. Robb, J. R. Cheeseman, G. Scalmani, V. Barone, B. Mennucci, G. A. Petersson, et al. Gaussian 09, Revision B.01; Gaussian, Inc.: Wallingford CT, 2010.
- 47 D. Zheng, X. Yuan and J. Ma, *Acta Physico-Chimica Sinica* 2016, **32**, 290-300.
- 48 C. Zhan and J. Yao, *Chem. Mater.*, 2016, **28**, 1948-1964.
- 49 B. Jiang, X. Zhang, C. Zhan, Z. Lu, Huang, J. X. Ding, S. He and J. Yao, *Polym. Chem.*, 2013, **4**, 4631-4638.
- 50 D. Núñez-Villanueva, G. Iadevaia, A. E. Stross, M. A. Jinks, J. A. Swain and C. A.

- J. Am. Chem. Soc.*, 2017, **139**, 6654-6662.
- 51 H. Adams, E. Chekmeneva, C. A. Hunter, M. C. Misuraca, C. Navarro, and S. M. Turega, *J. Am. Chem. Soc.*, 2013, **135**, 1853–1863.
- 52 S. Setayesh, A. C. Grimsdale, T. Weil, V. Enkelmann, K. Müllen, F. Meghdadi, E. J. List and G. Leising, *J. Am. Chem. Soc.*, 2001, **123**, 946-953.